Tunable Four-Port MIMO/Self-Multiplexing THz Graphene Patch Antenna with High Isolation

Mohd Farman Ali
National Institute of Technology Patna
Rajarshi Bhattacharya (rajarshi@nitp.ac.in)
National Institute of Technology Patna https://orcid.org/0000-0002-8530-2678
Gaurav Varshney
National Institute of Technology Patna

Research Article

Keywords: Graphene, MIMO, self-multiplexing, terahertz

Posted Date: March 8th, 2022

DOI: https://doi.org/10.21203/rs.3.rs-1414627/v1

Tunable Four-Port MIMO/Self-Multiplexing THz Graphene Patch Antenna with High Isolation

Mohd Farman Ali[1], Rajarshi Bhattacharya[2], and Gaurav Varshney[3]

Department of ECE, National Institute of Technology Patna, Patna−800005, India

farman.nitp@gmail.com[1], r.b.1980@ieee.org[2], gaurav.ec@nitp.ac.in[3]

***Abstract*— A tunable terahertz four-port multiple-input-multiple-output (MIMO) graphene microstrip patch antenna with self-multiplexing ability is designed and numerically studied. The top layer of the four-port patch antenna, which is a symmetric cross-shaped graphene patch, is patterned using a cross-slot. Insertion of this cross-slot improved the level of isolation to the order of 50−70 dB in the MIMO mode of operation. The frequency of impedance matching at each port of the designed antenna could be tuned independently by applying an electrostatic potential on the corresponding graphene patch enabling its usage as a MIMO self-diplexing and quadruplexing antenna. The MIMO performance parameters like envelope correlation coefficient, diversity gain, mean effective gain, etc. are found within the acceptable limits. An equivalent circuit model is presented to provide insight into the radiation mechanism and validate the results.**

***Index Terms*-- Graphene, MIMO, self-multiplexing, terahertz.**

1. Introduction

The terahertz (THz) frequency ranging from 0.1 to 10 THz with wavelength ranging from 3 mm to 30 μm is being explored owing to its capability in providing the wide bandwidth, high data rates, and high-speed miniaturised processing for future communication systems (Akyildiz et al. 2014). In this context, antennas design for THz communication is under consideration for quite some time (Abadal et al. 2019; Akyildiz and Jornet 2016; Dash et al. 2022; Faisal et al. 2020; Hosseininejad et al. 2019; Hosseininejad et al. 2017; Sarieddeen et al. 2019; Xu et al. 2014). The multiple-input-multiple-output (MIMO) communication and antenna design for the same is being emphasized for increasing the data rate since inception of the massive MIMO and millimeter wave (mm-wave) beamforming concepts, which is extended to the THz frequency range as well (Akyildiz and Jornet 2016; Faisal et al. 2020; Sarieddeen et al. 2019), (Ali et al. 2021; Ali et al. 2020; Das et al. 2021; Esfandiyari et al. 2019; Luo et al. 2019; Malhat et al. 2022; Shamim et al. 2021; Temmar et al. 2021; Vijayalakshmi et al. 2021; Zhang et al. 2019). In many of these works, the massive MIMO antenna system is implemented with separate excitation of each radiator indicating implementation of fully digital beamforming (Akyildiz and Jornet 2016; Faisal et al. 2020;

Sarieddeen et al. 2019). A single unit multi-beam MIMO antenna with beam-reconfigurable is introduced in (Luo et al. 2019) for 5G and beyond applications. It is worth noting that the antennas reported in [10,15,16] do not offer tunability, which could be attended in micro/nano-scale devices if attempted with proper use of reconfigurable materials (Abdollahramezani et al. 2021; Dash et al. 2021; Narges Kiani, Farzad Tavakkol Hamedani and Rezaei 2021; Pascual et al. 2022; Sharma et al. 2020).

So far, the issue of mutual coupling reduction of RF MIMO antennas is investigated in-depth and various techniques like orthogonal placement of antennas (Maurya and Bhattacharya 2020), generation of orthogonal radiation pattern (Bhattacharya et al. 2016a; Bhattacharya et al. 2016b), usage of passive decoupling structure that provides alternative coupling path (Maurya et al. 2018; Maurya and Bhattacharya 2021), usage of metamaterial, etc. (Pan et al. 2016). The problem of mutual coupling reduction in THz graphene MIMO antennas is addressed in (Ali et al. 2021; Vijayalakshmi et al. 2021; Zhang et al. 2019). A graphene-based frequency selective surface (FSS) is used in (Zhang et al. 2019), where the structure becomes 3D and its fabrication becomes challenging, and a meandered line decoupling structure is used in (Vijayalakshmi et al. 2021) for enhancement of isolation. Recently, a tunable two-port THz MIMO antenna with the option of diplexing is reported in (Ali et al. 2021), where the isolation is achieved by inserting a slot on the graphene patch.

A MIMO antenna with multiplexing ability makes it more useful especially in the present-day multi-standard communication scenario. It is well known that usage of multiple transceivers often leads to undesired higher-order effects like intermodulation distortion (Kumar et al. 2020; Mukherjee and Biswas 2016). Multiplexer circuits such as diplexer, quadruplexer, etc. are used to do away with these problems by improving the isolation (Chuang and Wu 2011). The usage of a separate multiplexer circuit increases the overall size, complexity, and cost of the RF front-end. Therefore, a substantial amount of research is being carried out in designing compact ferrite-free antenna structures having self-multiplexing ability in the RF frequency range: self-diplexing antenna $\left(\left|S_{ij}\right| \approx -25\ dB\right)$ (Mukherjee and Biswas 2016), self-quadruplexing antenna $\left(\left|S_{ij}\right| \approx -25\ dB\right)$ (Kumar et al. 2020), and self-quadruplexing/MIMO antenna $\left(\left|S_{ij}\right| \approx -20\ dB\right)$ (Boukarkar and Lin 2020). To the best of the author's knowledge, no reconfigurable MIMO/self-quadrupling antenna, working in the THz band, is available in the literature.

In this era of increased cognitive ability in communication systems, frequency agility would be another desirable characteristic of THz MIMO self-multiplexing antennas (Kumar et al.

2018; Rajo-Iglesias et al. 2014; Ridwan et al. 2021). The tunability is possible at the millimetre scale dimension or the microwave frequency by using the varactor-diode, PIN-diode, and MEMS switches (Dai et al. 2020; Rajo-Iglesias et al. 2014). The THz developments are possible with the micro/nanoscale dimensions which do not allow the usage of these devices for obtaining tunability. In recent investigations, the advent of tunable bandgap materials is paving the way for the implementation of tunable THz devices. Graphene is one of the most promising 2D materials used in THz and mid-infrared frequency bands due to its unique electronic and optical properties (Choudhury and Abou El-Nasr 2017). The application of electrostatic field on the graphene material can tune its surface conductivity and hence the frequency response of graphene-based devices (Abadal et al. 2019).

In this work, a graphene-based tunable THz four-port proximity-coupled MIMO/self-multiplexing patch antenna is designed. A cross-shaped slot is introduced in the graphene-based radiator which improves the isolation, and it increases the port-to-port isolation by $25-30$ dB. The proposed antenna provides pattern diversity and can offer multi-directional coverage. The response of each radiating element through the individual port of the antenna can be tuned independently by applying an electrostatic DC bias voltage on the graphene patch. Thus, the designed antenna can offer the capability of self-diplexing and quadruplexing depending upon the value of the applied DC voltage on each radiator.

2. Antenna design

The 3D view and schematic of biasing mechanism of the proposed tunable four-port MIMO/self-multiplexing graphene patch antenna are shown in Fig. 1(a) and (b) respectively. The design evolution is depicted in Fig. 2. This graphene microstrip patch antenna is microstrip line fed. The proposed MIMO antenna consists of two silicon dioxide (SiO_2) substrates of heights h_1 and h_2, respectively, and it is being fed by proximity (see Fig. 1(a)). A cross-shaped patch of monolayer graphene of thickness $0.34\,nm$ is placed on the top of the upper substrate. Four ports are placed symmetrically as shown in Fig. 1. It is worth mentioning that the value of all the dimensions of the final design is given in the caption of Fig. 1. The length of the transmission line that goes under the patches and the height of the upper substrate (h_2) are decided such that the antenna remains low-profile while maintaining the impedance matching. Finally, four narrow corner-slots (with a slot width of

$g = 0.1\ \mu m$) are inserted symmetrically as shown in Fig. 1(a) in the final MIMO antenna to enable independent dc biasing of the four graphene patches as shown in Fig. 1(b).

In this work, the full-wave simulation of the graphene antennas is performed using CST microwave studio in the time domain. The monolayer graphene material is selected from the CST macros library. For the simulation, the parameters are considered as temperature, $T = 300K$, relaxation time, $\tau = 1\ ps$ and the value of chemical potential, μ_c can be selected in the range from 0 to 1 eV. In this paper, μ_c is taken as $0.16\ eV$ if not otherwise mentioned. Next, the design and analysis of Antenna-1, 2, and 3 are dealt with in detail in the following two subsections.

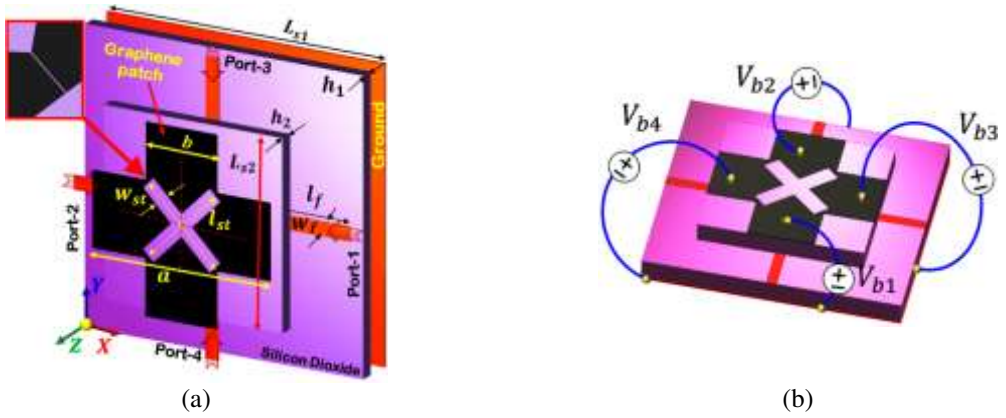

(a) (b)

Fig. 1 Antenna structure (a) perspective separated 3D view and (b) the electrostatic biasing mechanism of the radiators $L_{s1} = 56, L_{s2} = a = 36, h_1 = h_2 = 1.6, b = 14.5, l_{st} = 18.5, w_{st} = 4, l_f = 18$ and $w_f = 2$ dimensions unit μm). Four dc isolation slots of width $g = 0.1\ \mu m$ are carved at the four corners. The structure of this 4-port antenna is fully symmetric with respect to (*w.r.t.*) all the ports. Hence, the values of only the minimum required numbers of dimensions are only mentioned to keep the figure legible.

2.1. Design of Antenna-1

The top view of Antenna−1 is shown in Fig. 2(a). Notably, the cross-shaped graphene patch is continuous and there is not any slot. While designing Antenna-1, the main focus is given on impedance matching and modal configuration. It is shown in (Ali et al. 2021) that this kind of graphene patch antenna works as a cavity-backed surface plasmons polariton (SPP) radiator, where the transverse magnetic (TM) SPP modes propagate along the graphene patch (Balaban et al. 2013). The $TM_{\frac{1}{2}2}$ mode is excited in the arms of the cross-shaped graphene patch cavity, made of magnetic wall boundary conditions on three sides (see Fig. 3(a)) to obtain input impedance matching (Ali et al. 2021). The distribution of the magnitude of the

electric field on Antenna-1, shown in Fig. 3(a), depicts that the SPP can propagate in a relatively unperturbed manner when it reaches the central section of the cross-shaped graphene patch. Interestingly, the SPP leaky wave loses its energy over a short distance despite being successfully excited at the feed. The reflection coefficient of this symmetric MIMO antenna is shown in Fig. 4(a). This decay of the SPP is evident in Fig. 3(a) and its effect on the mutual coupling is shown in Fig. 4(b) and (c). Though no special care is taken in designing Antenna-1 to reduce the mutual coupling, the isolation remains on the order of 35−40 dB. Notably, the mutual coupling to the nearer ports is around 5 dB higher compared to the coupling to the port, lying on the opposite side.

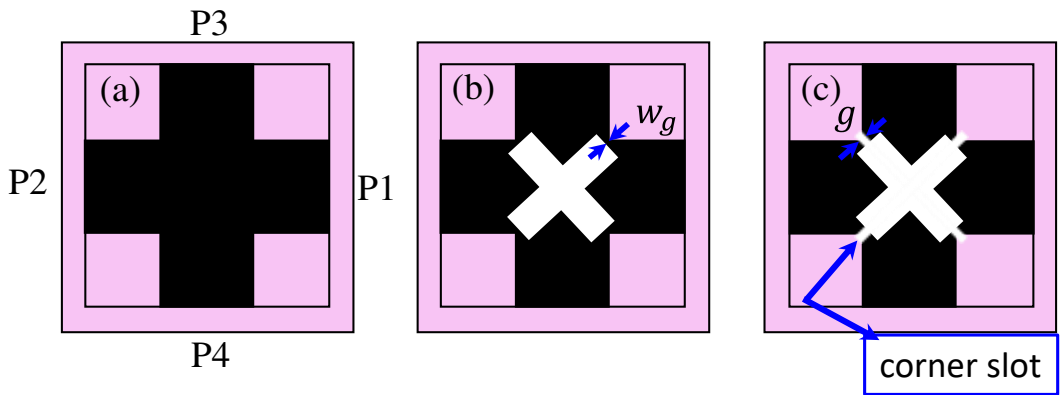

Fig. 2. The structure of (a) Antenna-1 (continuous graphene patch), (b) Antenna-2 (Antenna-1 with cross-slot) and (c) Antenna-3 (Antenna-2 with dc-isolation slot of width $g = 0.1\ \mu m$ at the corners)

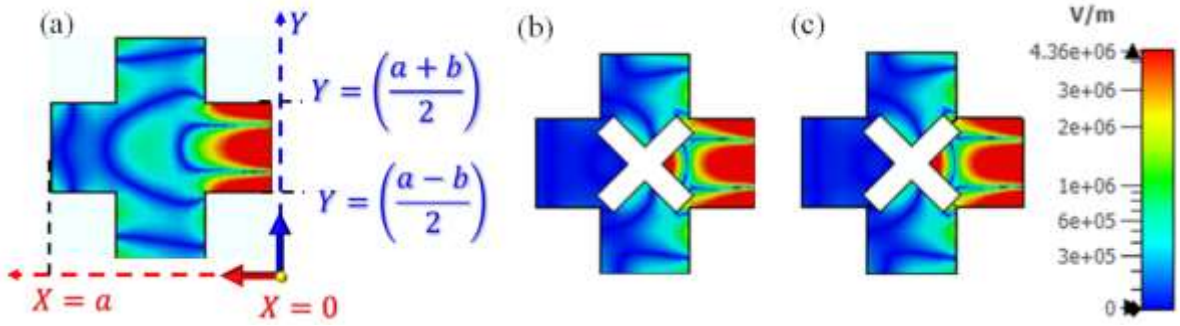

Fig. 3. The absolute electric field in the XY plane on the top surface of (a) Antenna-1, (b) Antenna-2, and (c) Antenna-3, when the port-1 is excited at frequency 1.76 THz and all other ports are terminated at matched load. [with $\mu_c = 0.16\ eV, \tau = 1\ ps, T = 300\ K$]

Graphene is known to have a relatively lower value of the real part of the conductivity $\left(Re\{\sigma_{Graphene}\}\right)$ compared to that of the highly conductive materials like silver, copper, etc. in the operating frequency range. Therefore, conduction loss is a concern in antennas made of graphene, a material with electrically reconfigurable conductivity, in the THz band. Here, an

interesting numerical experiment has been carried out to study the effect of $\sigma_{Graphene}$ on the return loss (RL) of Antenna-1. If the relaxation time (τ) of graphene is reduced, the scattering rate of the electrons increases and the value of $\sigma_{Graphene}$ reduces accordingly as per (1)−(4). In this regard, the value of τ is varied from $0.25-1.0\ ps$ with $\mu_c = 0.16\ eV$ in the CST full-wave simulation and the $|S_{11}|$ is plotted in Fig. 4(d). It is clearly evident from Fig. 4(d) that the impedance matching is gradually reduced and finally, totally lost when the $\sigma_{Graphene}$ is lowered by gradually reducing τ from 1 to 0.25. Therefore, the present design is rather immune to the problem of lowering RL at the cost of an increase in energy dissipation through $\frac{1}{2} Re\{\sigma\}|\boldsymbol{E}.\boldsymbol{E}^*|^2$.

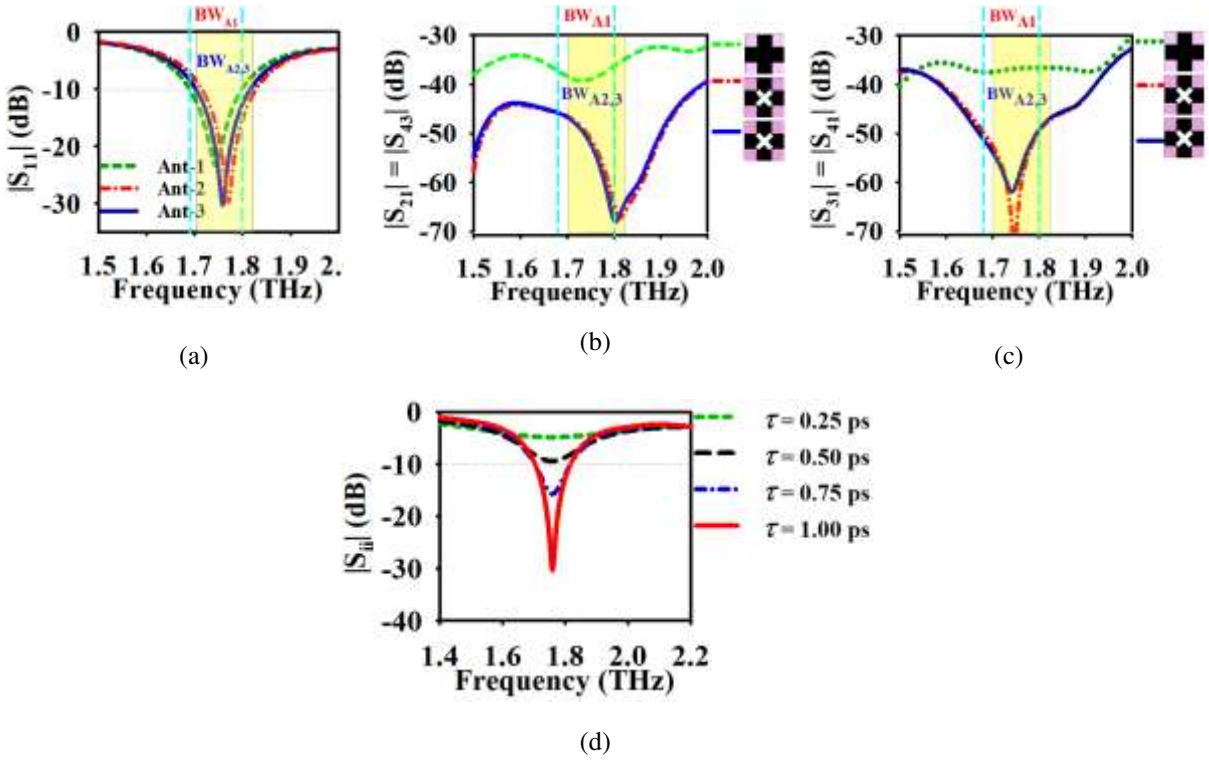

Fig. 4. The frequency response of (a) reflection coefficient $|\boldsymbol{S_{11}}| = |\boldsymbol{S_{22}}| = |\boldsymbol{S_{33}}| = |\boldsymbol{S_{44}}|$, (b) and (c) isolation between the ports of Antenna-1, 2 and 3 (BW_{A1}, $BW_{A2,3}$ -bandwidth of Antenna-1, 2 and 3, respectively), and (d) effect of relaxation time τ on impedance matching.

2.2. Design of Antenna-2 and 3

A cross-slot is engraved in Antenna-1 to reduce the mutual coupling between the ports, and it is named Antenna-2, as shown in Fig. 2(b). The dimension of the cross-slot, i.e., w_{st} and l_{st}, which in turn decides the width of the narrow gap (w_{gap}) at the corner, are selected such that *i*) the port-level impedance matching is not compromised and *ii*) mutual coupling to both the near and far ports are minimized. Finally, in the Antenna-3, four narrow corner-slots of width $g = 0.1\ \mu m$ are added on the graphene patch of Antenna-2 (see Fig. 1 and Fig. 2(c)) to

provide dc isolation between the adjacent graphene patches. It is also evident from (A.5), for the final design, the dc bias voltage V_{bi} of the i −th antenna controls the chemical potential (μ_{ci}) of only the i −th patch of the 4−port MIMO antenna due to the dc isolation, shown in Fig. 2(c). Thus, in the multiplexing mode, different dc biasing voltages could be applied to the different graphene patches (see Fig. 1(b)) due to this dc isolation. The $|S_{11}|$ plots of Fig. 4(a) shows that the impedance matching of Antenna-2 and 3 are retained approximately in the same band as Antenn-1 except for a slight increase in the resonant frequency. This shift could be attributed to the fact that incorporation of the cross slot on the graphene patch imposes magnetic walls, i.e., $\boldsymbol{n}.\boldsymbol{E} = 0$, and creates a rather confined resonant cavity as shown in Fig. 3(b) and (c). Thus, k_x of the $TM_{\frac{1}{2}2}$ mode excited in the pentagonal (from the top view of Fig. 3(b) and (c)) cavity is slightly increased compared to the same antenna shown in Fig. 3(a) resulting in a slight increase in the resonant frequency of the Antenna- 2, 3.

More importantly, the isolation between the ports is increased from the order 35−40 dB to the order of 60−70 dB as the result of the incorporation of the cross-slot. When the port-1 is excited and all the other ports are terminated at matched load, insertion of the cross-slot inhibits propagation of the SPP from Patch-1 to its neighbouring patches, viz., Patch-3 and 4, as depicted in the electric field distribution of Fig. 3 (b) and (c). Thereby, the field coupling to Patch-2 diminishes as well. To further investigate the background physics of reduction in the mutual coupling, we study the distribution of $\boldsymbol{E}$ and the corresponding magnetic surface current density ($\boldsymbol{M_s}$) on the cross-slot is presented in Fig. 5. The altered symmetry $\boldsymbol{M_s}$ in Patch-3 and 4, *w.r.t.* that of Patch-1 and 2, prohibits resonance of Patch-3, 4 at 1.76 THz and thereby reduces mutual coupling drastically.

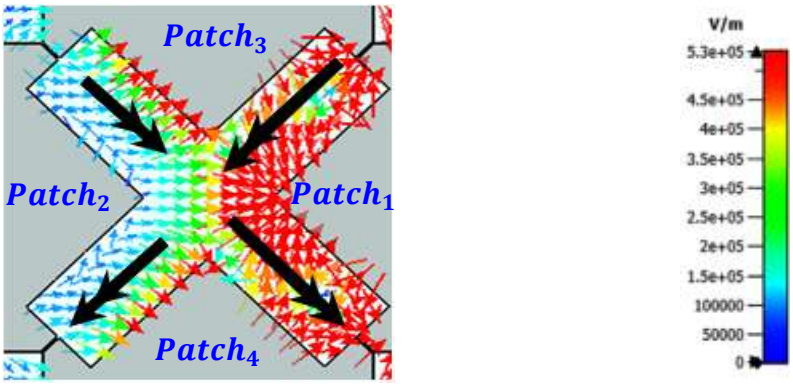

Fig. 5. The $\boldsymbol{E}$ field distribution on the cross-slot of the proposed 4-port MIMO antenna, i.e., antenna-3 at 1.76 THz. The colour bar is representing the electric field amplitude. An indicative distribution of the magnetic surface current density $\boldsymbol{M_s} = \boldsymbol{E} \times \boldsymbol{n}$ is shown with black arrows on the cross-slot.

3. Multiple functionalities of designed four-port antenna

Based on the applied electrostatic bias voltage of the different patches, the proposed antenna offers multiple functionalities. The multi-functionality of the designed antenna can be understood from Table-1. It can offer multifunctionality as *i*) tunable 4-port MIMO antenna, *ii*) Tunable self-Multiplexing. In self-multiplexing, self-diplexing and self-quadruplexing antenna depending upon the value of the applied gate voltage on the antenna structure (Fig. 1(b)). The multi-functionalities of the proposed antenna are defined in the following sub-sections.

Table-1 Antenna functionalities

S.N.	Applied bias voltage	Chemical potential on the graphene patches	Functionalities of the tunable four-port antenna
1	$V_{b1} = V_{b2} = V_{b3} = V_{b4}$	$\mu_{c1} = \mu_{c2} = \mu_{c3} = \mu_{c4} = \mu_c$	4-Port MIMO antenna
2	$(V_{b1} = V_{b2}) \neq (V_{b3} = V_{b4})$	$(\mu_{c1} = \mu_{c2}) \neq (\mu_{c3} = \mu_{c4})$	2-Port MIMO antenna with Self-**diplexing** ability
3	$V_{b1} \neq V_{b2} \neq V_{b3} \neq V_{b4}$	$\mu_{c1} \neq \mu_{c2} \neq \mu_{c3} \neq \mu_{c4}$	Self-**quadruplexing** antenna

3.1. Four-port MIMO antenna

For using the proposed antenna as a 4-port MIMO antenna, all the patches must resonate at the same frequency. Hence, the applied gate voltage at each port must be set at equal values as $V_{b1} = V_{b2} = V_{b3} = V_{b4}$. In this subsection first, an electrical circuit model (ECM) of this MIMO antenna is presented to obtain further insight into its working principle (Fig. 6(a) and (b)). Subsequently, the tunability of the designed antenna and its MIMO performance are discussed. The radiators are modelled as parallel R-L-C resonators with feed capacitance C_f. All the equivalent circuit parameters, their physical significance, and their values are summarized in Table-2. As per the distribution of $\boldsymbol{M_s}$, shown in Fig.5, the cross-slot, used here to reduce mutual coupling, is non-radiating in nature. Therefore, this slot is modelled as a coupling network having mutual inductance and capacitance between each radiator of the antenna as shown in Fig. 6(b). The mutual coupling of two near patches can be obtained by a series of $L_{cc} - C_g$ with parallel to the cross-slot capacitance $C_{m_{ij}}$, and for far patches, the mutual coupling is modelled as coupling capacitance $C_{m_{ij}}$. The values of the feeding capacitance c_f and parallel R-L-C resonators parameters are estimated at the resonant frequency in the technique given in (Garg et al. 2000). Moreover, the circuit element's values of the coupling network can be obtained by observing the behaviour of isolation between the ports (see Fig. 4(b) and (c)). The obtained ECM parameters are enlisted in Table-2. Fig. 6(c)

shows the S-parameters computed using ECM and CST microwave studio time-domain simulation to be in good agreement showing that the behaviour of electromagnetic field in radiation and mutual coupling, described here are consistent.

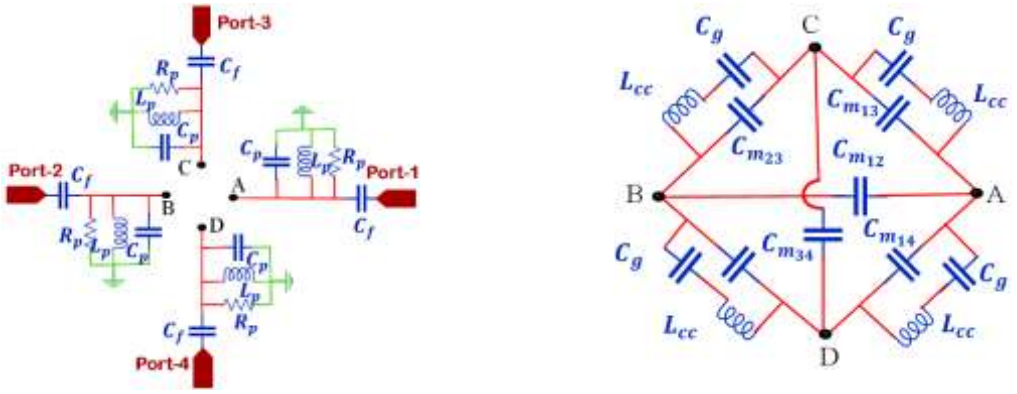

(a) (b)

Fig. 6. The lumped parameter circuit model of the proposed 4-port MIMO antenna (a) the ECM and (b) its coupling network

Table-2. ECM parameters of the 4-Port graphene patch antenna.

Ckt. Elements	Physical Significance	Values
R_p	Resistance of resonator	53 Ω
L_p	Inductance of resonator	0.0261 fH
C_p	Capacitance of resonator	2.12 pF
$C_{m_{ij}}$	Cross-slot Capacitance	2.50 fF
C_f	Feed capacitance of proximity coupled feed	8.46 fF
C_g	Corner slot gap capacitance	4.0 fF
L_{cc}	Inductance due to current crowding near the corner slots	2.045 nH

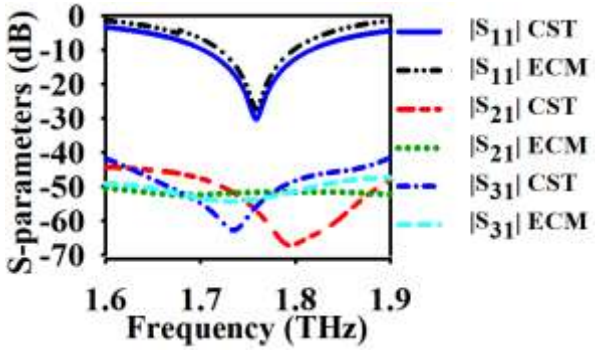

Fig. 7. Performance comparison of the ECM with CST full-wave simulation.

Regarding the tunability of the designed MIMO antenna, Fig. 8 depicts that impedance matching is obtained in the range of 1.65−2.1 THz by varying μ_c. Fig. 9 shows the simulated

3D directivity radiation pattern in a linear scale of the proposed MIMO antenna for two different values of chemical potentials the radiation pattern in Fig. 9(a) 1.76 THz ($\mu_c = 0.16\ eV$) and (b) at 2.08 THz ($\mu_c = 0.22\ eV$). The beam-tilting is known to be due to the leaky nature of SPP (Ali et al. 2020; Correas-Serrano et al. 2014; Esquius-Morote et al. 2014). The envelope correlation coefficient (ECC), denoted by ρ_{ij}, is an important parameter for MIMO antenna design. The value of ECC is measured from the 3D far-field radiation pattern in the receiving mode of antenna operation (Ali et al. 2021). The proposed antenna gives better-simulated results on certain conditions like XPR = 2, uniform Gaussian distribution with 0° mean and 10° variance. For ports-1 and 2, the ECC $\rho_{12} > 0.046$ and ports-1 and 3 the $\rho_{13} > 0.0086$ (Maurya and Bhattacharya 2020). Another parameter is diversity gain (DG) which also relates to ECC. The DG for ports-1 and 2, DG > 9.985 and for ports-3 and 4 DG > 9.999. Also, the mean effective gain of the proposed antenna at each port remains around -3 dB.

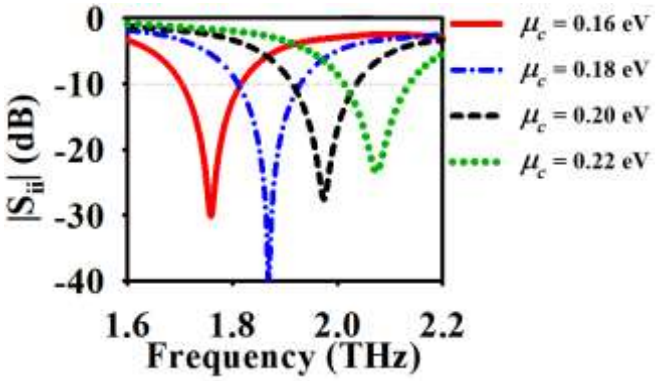

Fig. 8. Tunability in $|S_{ii}|, i = 1,2,3,$ and 4 of the symmetric MIMO antenna for different values of the chemical potential.

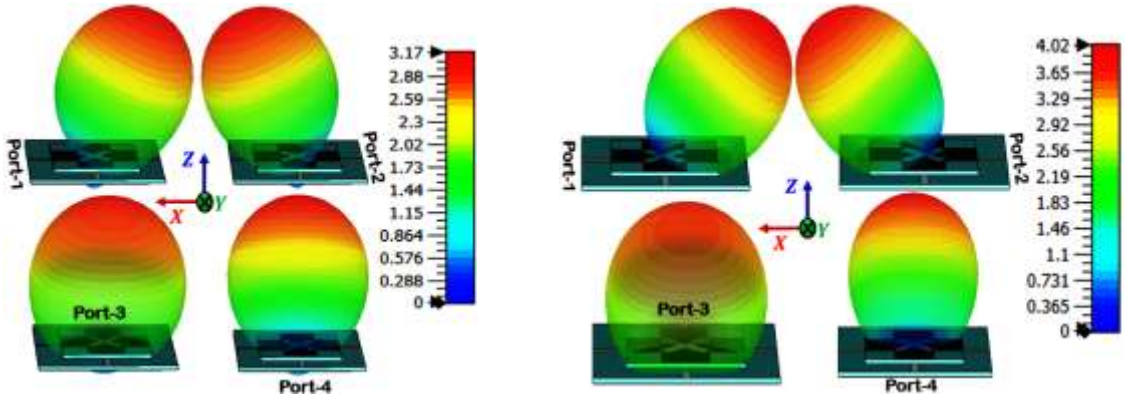

(a) (b)

Fig. 9. 3D radiation pattern of the proposed MIMO antenna in linear scale (a) at frequency 1.76 THz with $\mu_c = 0.16\ eV$, and (b) at frequency 2.08 THz with the, $\mu_c = 0.22\ eV$ with the excitation of different ports.

3.2. Self-multiplexing antenna

Table-2 shows that apart from being used as a MIMO antenna, the designed quad-port antenna could be used as a self-multiplexing antenna, where a good amount of hardware could be avoided. The independent tunability, elaborated in (Ali et al. 2020) for two-port graphene patch antenna, of the proposed MIMO antenna ports can be utilized to obtain the different types of self-multiplexing antenna characteristics. This antenna can offer mainly *i*) 2-Port MIMO antenna with the self-diplexing ability and *ii*) 4-port self-quadruplexing ability as detailed in the following two subsections. However, it is worth mentioning that a self-triplexing option is also available in the designed antenna.

3.2.1. 2-Port MIMO antenna with self-diplexing ability

In the 2-port MIMO diplexing mode, any two bias voltages are set at equal value as with one of the possible combinations $(V_{b1} = V_{b2}) \neq (V_{b3} = V_{b4})$. Fig. 10(a) depicts the S-parameters of the antenna offering the self-diplexing capability. The antenna operates at two different frequencies, viz. a lower frequency of 1.76 THz and a higher frequency of 2.35 THz. Fig. 10(b) shows the isolation between the ports which is better than 35 dB in the operating passband. The isolation levels in the two frequency bands of 1.76 THz and 2.35 THz are summarized in Table-3.

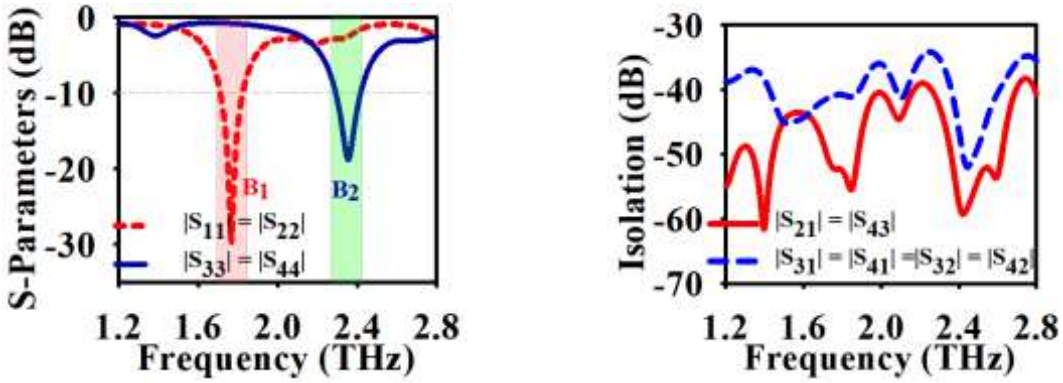

(a) (b)

Fig. 10. The frequency response of (a) reflection coefficients, (b) isolation when the antenna offers the self-diplexing/MIMO functionality with $\mu_{c1} = \mu_{c2} = 0.16\ eV,\ \mu_{c3} = \mu_{c4} = 0.28\ eV$.

Table-3. Summary of mutual coupling levels in the self-diplexing mode.

Frequency Band	Max. of $\|S_{ij}\| = \|S_{ji}\|\ dB$ (Between two antennas at the opposite sides)		Max. of $\|S_{ij}\| = \|S_{ji}\| dB$ (Between placed antennas side-by-side)	
B_1 $(1.71 - 1.82\ THz)$	$i = 1$ $j = 2$	-52.6	$i = 1\ or\ 2$ $j = 3\ or\ 4$	-40.4
B_2 $(2.29 - 2.41\ THz)$	$i = 3$ $j = 4$	-41.8	$i = 3\ or\ 4$ $j = 1\ or\ 2$	-35.1

3.2.2. 4-Port self-diplexing antenna

For the self-quadruplexing mode of operation, all the applied bias voltages are required to be set at different values $V_{b1} \neq V_{b2} \neq V_{b3} \neq V_{b4}$ so that the corresponding antennas work at different frequencies. Fig. 11 shows the S-parameters and the input impedance of the antenna with its functionality as a self-quadruplexing antenna. With the application of the different dc bias voltages, the antenna operates at the resonant frequencies 1.76, 2.08, 2.35, and 2.60 THz corresponding to the values of chemical potential as $\mu_{c1} = 0.16\ eV$, $\mu_{c2} = 0.22\ eV$, $\mu_{c3} = 0.28\ eV$ and $\mu_{c4} = 0.34\ eV$, respectively. The isolation between the ports remains more than 30 dB in the case of antenna function as a self-quadruplexing antenna. The isolation levels in the four frequency bands, mentioned above, are summarized in Table-4.

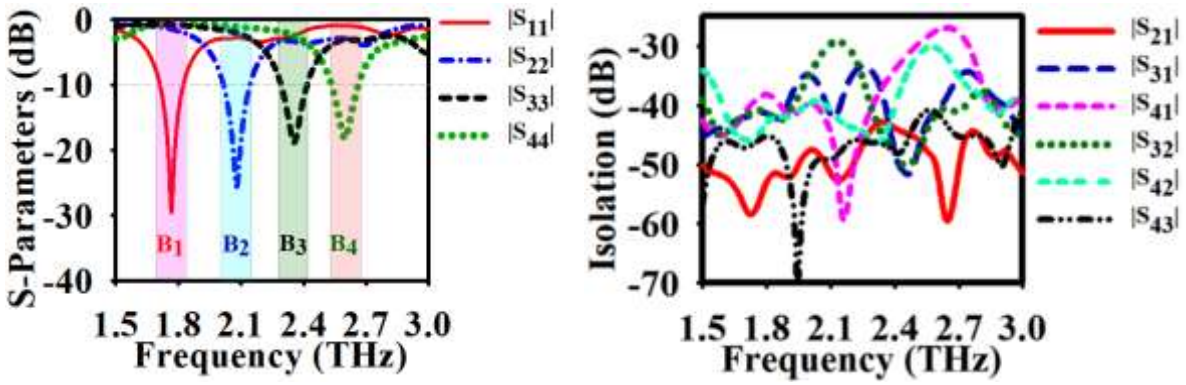

(a) (b)

Fig. 11. The frequency response of (a) reflection coefficients and (b) isolation with the functionality of antennas as a self-quadruplexing antenna with $\mu_{c1} = 0.16\ eV, \mu_{c2} = 0.22\ eV, \mu_{c3} = 0.28\ eV$, and $\mu_{c4} = 0.34\ eV$.

Table-4. Summary of mutual coupling levels in the quadruplexing mode.

Frequency Band	Max. of $\lvert S_{ji} \rvert\ dB$ (Between two antennas at the opposite sides)		Max. of $\lvert S_{ji} \rvert\ dB$ (Between placed antennas side-by-side)	
B_1 $(1.71 - 1.82\ THz)$	$i = 1$ $j = 2$	-51.8	$i = 1$ $j = 3, 4$	$-42, -41.8$
B_2 $(2.02 - 2.15\ THz)$	$i = 2$ $j = 1$	-46.5	$i = 2$ $j = 3, 4$	$-38.8, -41$
B_3 $(2.29 - 2.42\ THz)$	$i = 3$ $j = 4$	-46	$i = 3$ $j = 1, 2$	$-35.1, -33.3$
B_4 $(2.54 - 2.67\ THz)$	$i = 4$ $j = 3$	-43.5	$i = 4$ $j = 1, 2$	$-40.5, -31.0$

A comparative study of the proposed antenna with the others, available in the literature, in terms of MIMO performance, is reported in Table-5. It shows that the proposed antenna offers an increased number of ports with tunable frequency response. The designed antenna provides the smallest value of ECC and the highest value of the isolation between the ports.

However, it is worth reiterating that the proposed four-port reconfigurable MIMO antenna offers the capability of self-multiplexing as well. According to the results, summarized in Table- 3 and 4, the isolation levels attained in the designed antenna are better than the ones reported in (Boukarkar and Lin 2020; Kumar et al. 2020; Mukherjee and Biswas 2016).

Table-5. State-of-the-art comparison as MIMO antenna.

Ref.	No. of Ports	Material	Size of the antenna ($\mu m \times \mu m$)	Resonance Frequency (THz)	Isolation Enhancement Techniques	Frequency Tunability	Max. ECC	Min. Isolation (dB)	Operating Mode
(Esfandiyari et al. 2019)	2-port	Copper on Pyrex	380 × 380	1.1	Metamaterial	No	–	20	MIMO
(Zhang et al. 2019)	4-port	Graphene on SiO_2	84 × 84	1.16, 1.41	FSS	Yes	0.01	25	MIMO
(Ali et al. 2021)	2-port	Graphene on SiO_2	60 × 40	1.68 &1.81	slot	Yes	0.17	40	Self-diplexing with MIMO
(Vijayalakshmi et al. 2021)	2-port	Graphene on Polyimide	50 × 40	2.3, 3.2, & 4.5	Decoupling Structure	No	0.2	15	MIMO
(Das et al. 2021)	4-port	Copper on polyimide	125 × 125	Wideband	–	No	0.02	20	MIMO
(Temmar et al. 2021)	2-port	Graphene on Polyimide	600×600	0.65	–	Yes	–	30	MIMO
Proposed work	**4-port**	**Graphene on SiO_2**	**56×56**	**1.76**	**Cros slot**	**Yes**	**0.0086**	**50−70**	**MIMO with Self-multiplexing Ability**

4. Conclusion

A tunable terahertz four-port MIMO antenna has been designed and numerically studied. A technique has been implemented for improving the isolation between the ports of the THz MIMO antenna. The isolation between the ports has been obtained up to the level of 50 to 70 dB with the usage of the applied technique of carving a cross-shaped slot in the graphene radiator. The independent tunability through each port has been achieved by applying an electrostatic voltage on the graphene-based radiator. The functionality of the proposed antenna as with the capability of self-diplexing and quadruplexing has been verified with the numerical simulations. The antenna provides 6.81% (1.70-1.82 THz) 10 dB impedance bandwidth with a minimum of 50 dB isolation in the passband. It can also be used as MIMO with STAR ability antenna for THz communications. The MIMO performance parameters like ECC, $\rho_{12} > 0.046$, $\rho_{13} > 0.0082$, DG ≥ 9.989, and MEG > -3 dB are calculated and found within the acceptable limits.

Appendix-1 Conductivity mode of graphene

The surface conductivity of graphene can be tuned by applying an external gate voltage. The surface conductivity of graphene has intraband and interband parts (Hanson 2008). In the lower THz frequency regime, the intraband part of the surface conductivity remains dominant with the insignificant value of the interband part (Hanson 2008). The intraband part of the surface conductivity of graphene by Kubo formalism is given in (A.1).

$$\sigma_{Graphene} = -j\frac{q_e^2 k_B T}{\Pi\, \hbar^2(\omega - j2\Gamma)}\left[\frac{\mu_c}{k_B T} + 2\, ln\left(1 + \exp\left(-\frac{\mu_c}{k_B T}\right)\right)\right] \tag{A-1}$$

$$\tau = \frac{\mu_c \mu_g}{q_e v_f^2} \tag{A.2}$$

$$n_s = \frac{2}{\pi\hbar^2 v_f^2}\int_0^\infty E\big(f_d(E) - f_d(E + 2\mu_c)\big)\, dE, \tag{A.3}$$

where,

$$f_d(E) = \left(1 + \exp\left(\frac{E - \mu_c}{k_B T}\right)\right)^{-1} \tag{A.4}$$

Here, $q_e, \omega, \hbar, k_B, \mu_c, T$ are the electronic charge, frequency of operation, reduced Planck's constant, Boltzmann's constant, chemical potential, and temperature, respectively. In (A.1), Γ is the rate of scattering of electrons in graphene with relaxation time $\tau = 1/2\Gamma$, defined in (A.2), where μ_g is the mobility of graphene and v_f is the Fermi velocity. The carrier density n_s is defined in (A.3), where E is the total energy and $f_d(E)$, defined in (A.4), is the Fermi-Dirac distribution function. In the case of graphene Fermi energy, generally known as chemical potential, could be varied easily by simply providing electrostatic bias as given in (A.5). The chemical potential of each graphene patch can be dynamically tuned by applying a dc bias voltage. For the designed proximity coupled multilayered structure, the electrostatic dc bias voltage of graphene patches can be obtained in terms of chemical potential by extending the standard relation (Ali et al. 2021)

$$V_{bi} = \frac{q_e \mu_{ci}^2 (h_1 + h_2)}{\pi\hbar^2 v_f^2 \epsilon_o \epsilon_r}, \;\; i = 1,2,3,4. \tag{A.5}$$

Declarations

Funding: No funds, grants, or other support was received.

Data availability: The datasets generated during and/or analysed during the current study are available from the corresponding author on reasonable request.

Conflict of interest: The authors declare that there is no conflict of interest/competing interests related to this submission.

References

Abadal, S., Hosseininejad, S.E., Lemme, M., Bolivar, P.H., Solé-Pareta, J., Alarcón, E., Cabellos-Aparicio, A.: Graphene-Based Antenna Design for Communications in the Terahertz Band. Nanoscale Netw. Commun. Handb. 25–45 (2019). https://doi.org/10.1201/9780429163043-2

Abdollahramezani, S., Hemmatyar, O., Taghinejad, M., Taghinejad, H., Krasnok, A., Eftekhar, A.A., Teichrib, C., Deshmukh, S., El-Sayed, M., Pop, E., Wuttig, M., Alu, A., Cai, W., Adibi, A.: Electrically driven programmable phase-change meta-switch reaching 80% efficiency. arXiv Prepr. arXiv2104. 10381 (2021)

Akyildiz, I.F., Jornet, J.M.: Realizing Ultra-Massive MIMO (1024×1024) communication in the (0.06-10) Terahertz band. Nano Commun. Netw. 8, 46–54 (2016). https://doi.org/10.1016/j.nancom.2016.02.001

Akyildiz, I.F., Jornet, J.M., Han, C.: Terahertz band: Next frontier for wireless communications. Phys. Commun. 12, 16–32 (2014). https://doi.org/10.1016/j.phycom.2014.01.006

Ali, M.F., Bhattacharya, R., Varshney, G.: Graphene-based tunable terahertz self-diplexing/MIMO-STAR antenna with pattern diversity. Nano Commun. Netw. 30, 100378 (2021). https://doi.org/10.1016/j.nancom.2021.100378

Ali, M.F., Singh, R.K., Bhattacharya, R.: Re-configurable graphene-based two port dual-band and MIMO antenna for THz applications. 2020 IEEE Students' Conf. Eng. Syst. SCES. 4–8 (2020). https://doi.org/10.1109/SCES50439.2020.9236760

Balaban, M. V., Vukovic, A., Benson, T.M., Nosich, A.I.: Accurate numerical study of graphene disk surface plasmon resonances. 2013 IEEE 33rd Int. Sci. Conf. Electron. Nanotechnology, ELNANO 2013 - Conf. Proc. 73–75 (2013). https://doi.org/10.1109/ELNANO.2013.6552077

Bhattacharya, R., Garg, R., Bhattacharyya, T.K.: Design of a PIFA-Driven Compact Yagi-Type Pattern Diversity Antenna for Handheld Devices. IEEE Antennas Wirel. Propag. Lett. 15, 255–258 (2016)(a). https://doi.org/10.1109/LAWP.2015.2440260

Bhattacharya, R., Garg, R., Bhattacharyya, T.K.: A compact Yagi-Uda type pattern diversity antenna driven by CPW-fed pseudomonopole. IEEE Trans. Antennas Propag. 64, 25–32 (2016)(b). https://doi.org/10.1109/TAP.2015.2499756

Boukarkar, A., Lin, X.Q.: Miniaturized frequency-tunable self- quadruplexing four-element MIMO antenna system. IET Microwaves, Antennas Propag. 14, 973–979 (2020). https://doi.org/10.1049/iet-map.2020.0065

Choudhury, P.K., Abou El-Nasr, M.: Current trends of graphene technology. J. Electromagn. Waves Appl. 31, 1971–1973 (2017). https://doi.org/10.1080/09205071.2017.1388629

Chuang, M., Wu, M.: Microstrip Diplexer Design Using Common T-Shaped Resonator. IEEE Trans. Microw. Theory Tech. 21, 583–585 (2011)

Correas-Serrano, D., Gomez-Diaz, J.S., Alvarez-Melcon, A.: On the influence of spatial dispersion on the performance of graphene-based plasmonic devices. IEEE Antennas Wirel. Propag. Lett. 13, 345–348 (2014). https://doi.org/10.1109/LAWP.2014.2305836

Dai, L., Renzo, M. Di, Chae, C.B., Hanzo, L., Wang, B., Wang, M., Yang, X., Tan, J., Bi, S., Xu, S., Yang, F., Chen, Z.: Reconfigurable Intelligent Surface-Based Wireless Communications: Antenna Design, Prototyping, and Experimental Results. IEEE Access. 8, 45913–45923 (2020). https://doi.org/10.1109/ACCESS.2020.2977772

Das, S., Mitra, D., Bhadra Chaudhuri, S.R.: Fractal loaded planar Super Wide Band four element MIMO antenna for THz applications. Nano Commun. Netw. 30, 100374 (2021). https://doi.org/10.1016/j.nancom.2021.100374

Dash, S., Psomas, C., Krikidis, I., Akyildiz, I.F., Pitsillides, A.: Active Control of THz Waves in Wireless Environments using Graphene-based RIS. IEEE Trans. Antennas Propag. 1–14 (2022).

https://doi.org/10.1109/tap.2022.3142272

Dash, S., Soni, G., Patnaik, A., Liaskos, C., Pitsillides, A., Akyildiz, I.F.: Switched-Beam Graphene Plasmonic Nanoantenna in the Terahertz Wave Region. Plasmonics. 16, 1855–1864 (2021). https://doi.org/10.1007/s11468-021-01449-y

Esfandiyari, M., Jarchi, S., Ghaffari-Miab, M.: Channel capacity enhancement by adjustable graphene-based MIMO antenna in THz band. Opt. Quantum Electron. 51, 137 (2019). https://doi.org/10.1007/s11082-019-1856-2

Esquius-Morote, M., Gomez-Diaz, J.S., Perruisseau-Carrier, J.: Sinusoidally modulated graphene leaky-wave antenna for electronic beamscanning at THz. IEEE Trans. Terahertz Sci. Technol. 4, 116–122 (2014). https://doi.org/10.1109/TTHZ.2013.2294538

Faisal, A., Sarieddeen, H., Dahrouj, H., Al-naffouri, T.Y., Alouini, M.: Ultramassine MIMO Systems at Terahertz Bands Prospects and Challenges. IEEE Veh. Technol. Mag. 15, 33–42 (2020)

Garg, R., Bhartia, P., Ittipiboon, A.: Microstrip Antenna Design Handbook. Artech house (2000)

Hanson, G.W.: Dyadic green's functions for an anisotropic, non-local model of biased graphene. IEEE Trans. Antennas Propag. 56, 747–757 (2008). https://doi.org/10.1109/TAP.2008.917005

Hosseininejad, S.E., Alarcón, E., Komjani, N., Abadal, S., Lemme, M.C., Haring Bolívar, P., Cabellos-Aparicio, A.: Study of hybrid and pure plasmonic terahertz antennas based on graphene guided-wave structures. Nano Commun. Netw. 12, 34–42 (2017). https://doi.org/10.1016/j.nancom.2017.03.002

Hosseininejad, S.E., Rouhi, K., Neshat, M., Cabellos-Aparicio, A., Abadal, S., Alarcon, E.: Digital metasurface based on graphene: An application to beam steering in terahertz plasmonic antennas. IEEE Trans. Nanotechnol. 18, 734–746 (2019). https://doi.org/10.1109/TNANO.2019.2923727

Kumar, A., Saha, S., Bhattacharya, R.: Wavelet transform based novel edge detection algorithms for wideband spectrum sensing in CRNs. AEU - Int. J. Electron. Commun. 84, 100–110 (2018). https://doi.org/10.1016/j.aeue.2017.11.024

Kumar, K., Priya, S., Dwari, S., Mandal, M.K.: Self-Quadruplexing Circularly Polarized SIW Cavity-Backed Slot Antennas. IEEE Trans. Antennas Propag. 68, 6419–6423 (2020)

Luo, Y., Zeng, Q., Yan, X., Wu, Y., Lu, Q., Zheng, C., Hu, N., Xie, W., Zhang, X.: Graphene-based Multi-beam Reconfigurable THz Antennas. IEEE Access. 7, 30802–30808 (2019). https://doi.org/10.1109/ACCESS.2019.2903135

Malhat, H.A.E.A., Ghazi, A.M., Zainud-Deen, S.H.: Reconfigurable Multi-beam On-Chip Patch Antenna Using Plasmonics Parasitic Graphene Strip Array. Plasmonics. 17, 349–359 (2022). https://doi.org/10.1007/s11468-021-01532-4

Maurya, N.K., Bhattacharya, R.: Design of compact dual-polarized multiband MIMO antenna using near-field for IoT. AEU - Int. J. Electron. Commun. 117, 153091 (2020). https://doi.org/10.1016/j.aeue.2020.153091

Maurya, N.K., Bhattacharya, R.: CPW-Fed Dual-Band Compact Yagi-Type Pattern Diversity Antenna for LTE and WiFi. Prog. Electromagn. Res. C. 107, 183–201 (2021). https://doi.org/10.2528/PIERC20090905

Maurya, N.K., Tulsyan, M., Bhattacharya, R., Kumar, A.: Design and near field analysis of compact CPW-fed printed pseudo-monopole driven Yagi-type pattern diversity antenna. Appl. Electromagn. Conf. AEMC 2017. 2018-Janua, 1–2 (2018). https://doi.org/10.1109/AEMC.2017.8325742

Mukherjee, S., Biswas, A.: Design of Self-Diplexing Substrate Integrated Waveguide Cavity-Backed Slot Antenna. IEEE Antennas Wirel. Propag. Lett. 15, 1775–1778 (2016). https://doi.org/10.1109/LAWP.2016.2535169

Narges Kiani, Farzad Tavakkol Hamedani, P., Rezaei: Polarization controlling plan in graphene-based reconfigurable microstrip patch antenna. Opt. - Int. J. Light Electron Opt. 1–17 (2021). https://doi.org/10.1016/j.ijleo.2021.167595

Pan, B.C., Tang, W.X., Qi, M.Q., Ma, H.F., Tao, Z., Cui, T.J.: Reduction of the spatially mutual coupling between dual-polarized patch antennas using coupled metamaterial slabs. Sci. Rep. 6, 1–8 (2016). https://doi.org/10.1038/srep30288

Pascual, A.J., Ali, M., Batte, T., Ferrero, F., Brochier, L., de Sagazan, O., van Dijk, F., Munoz, L.E.G., Barrio, G.C. Del, Sauleau, R., Gonzalez-Ovejero, D.: Photonic-Enabled Beam Switching Mm-Wave Antenna Array. J.

Light. Technol. 40, 632–639 (2022). https://doi.org/10.1109/JLT.2021.3124092

Rajo-Iglesias, E., Tawk, Y., Costantine, J., Christodoulou, C.G.: Wireless corner: Cognitive-radio and antenna functionalities: A tutorial. IEEE Antennas Propag. Mag. 56, 231–243 (2014). https://doi.org/10.1109/MAP.2014.6821791

Ridwan, M.A., Radzi, N.A.M., Abdullah, F., Jalil, Y.E.: Applications of Machine Learning in Networking: A Survey of Current Issues and Future Challenges. IEEE Access. 9, 52523–52556 (2021). https://doi.org/10.1109/ACCESS.2021.3069210

Sarieddeen, H., Alouini, M.S., Al-Naffouri, T.Y.: Terahertz-Band Ultra-Massive Spatial Modulation MIMO. IEEE J. Sel. Areas Commun. 37, 2040–2052 (2019). https://doi.org/10.1109/JSAC.2019.2929455

Shamim, S.M., Das, S., Hossain, M.A., Madhav, B.T.P.: Investigations on Graphene-Based Ultra-Wideband (UWB) Microstrip Patch Antennas for Terahertz (THz) Applications. Plasmonics. 16, 1623–1631 (2021). https://doi.org/10.1007/s11468-021-01423-8

Sharma, G., Lakhtakia, A., Bhattacharyya, S., Jain, P.K.: Magnetically tunable metasurface comprising InAs and InSb pixels for absorbing terahertz radiation. Appl. Opt. 59, 9673–9680 (2020). https://doi.org/10.1364/AO.405023

Temmar, M.N.E., Hocini, A., Khedrouche, D., Denidni, T.A.: Analysis and design of MIMO indoor communication system using terahertz patch antenna based on photonic crystal with graphene. Photonics Nanostructures - Fundam. Appl. 43, 100867 (2021). https://doi.org/10.1016/j.photonics.2020.100867

Vijayalakshmi, K., Selvi, C.S.K., Sapna, B.: Novel tri-band series fed microstrip antenna array for THz MIMO communications, (2021)

Xu, Z., Dong, X., Bornemann, J.: Design of a reconfigurable MIMO system for THz communications based on graphene antennas. IEEE Trans. Terahertz Sci. Technol. 4, 609–617 (2014). https://doi.org/10.1109/TTHZ.2014.2331496

Zhang, B., Jornet, J.M., Akyildiz, I.F., Wu, Z.P.: Mutual Coupling Reduction for Ultra-Dense Multi-Band Plasmonic Nano-Antenna Arrays Using Graphene-Based Frequency Selective Surface. IEEE Access. 7, 33214–33225 (2019). https://doi.org/10.1109/ACCESS.2019.2903493